ChemPubSoc Europe

DOI: 10.1002/chem.201304012

CHEMISTRY A European Journal Full Paper

Rhenium Complexes

A Deadly Organometallic Luminescent Probe: Anticancer Activity of a Re^{I} Bisquinoline Complex

Igor Kitanovic,[a] Suzan Can,[a] Hamed Alborzinia,[a] Ana Kitanovic,[a] Vanessa Pierroz,[b, c] Anna Leonidova,[b] Antonio Pinto,[d] Bernhard Spingler,[b] Stefano Ferrari,[c] Roberto Molteni,[e] Andreas Steffen,*[e] Nils Metzler-Nolte,*[d] Stefan Wölfl,*[a] and Gilles Gasser*[b]

Abstract: The photophysical properties of $[Re(CO)_3(L\text{-}N_3)]Br$ ($L\text{-}N_3$ = 2-azido-*N*,*N*-bis[(quinolin-2-yl)methyl]ethanamine), which could not be localized in cancer cells by fluorescence microscopy, have been revisited in order to evaluate its use as a luminescent probe in a biological environment. The Re^{I} complex displays concentration-dependent residual fluorescence besides the expected phosphorescence, and the nature of the emitting excited states have been evaluated by DFT and time-dependent (TD) DFT methods. The results show that fluorescence occurs from a ^{1}LC/MLCT state, whereas phosphorescence mainly stems from a ^{3}LC state, in contrast to previous assignments. We found that our luminescent probe, $[Re(CO)_3(L\text{-}N_3)]Br$, exhibits an interesting cytotoxic activity in the low micromolar range in various cancer cell lines. Several biochemical assays were performed to unveil the cytotoxic mechanism of the organometallic Re^{I} bisquinoline complex. $[Re(CO)_3(L\text{-}N_3)]Br$ was found to be stable in human plasma indicating that $[Re(CO)_3(L\text{-}N_3)]Br$ itself and not a decomposition product is responsible for the observed cytotoxicity. Addition of $[Re(CO)_3(L\text{-}N_3)]Br$ to MCF-7 breast cancer cells grown on a biosensor chip micro-bioreactor immediately led to reduced cellular respiration and increased glycolysis, indicating a large shift in cellular metabolism and inhibition of mitochondrial activity. Further analysis of respiration of isolated mitochondria clearly showed that mitochondrial respiratory activity was a direct target of $[Re(CO)_3(L\text{-}N_3)]Br$ and involved two modes of action, namely increased respiration at lower concentrations, potentially through increased proton transport through the inner mitochondrial membrane, and efficient blocking of respiration at higher concentrations. Thus, we believe that the direct targeting of mitochondria in cells by $[Re(CO)_3(L\text{-}N_3)]Br$ is responsible for the anticancer activity.

Introduction

A current challenge in drug discovery is the enlargement of the available chemical space. Such an extension would increase the repertoire of chemical compounds whose biological activity could be screened. It can be anticipated that novel lead structures potentially useful for the pharmaceutical industry will be unveiled. A possible solution to enlarge this database is the investigation of poorly studied or even entirely new chemical structures. A class of compounds that has undoubtedly received little attention from the pharmaceutical industry is organometallic complexes. The skepticism towards

[a] *Dr. I. Kitanovic, S. Can, Dr. H. Alborzinia, Dr. A. Kitanovic, Prof. Dr. S. Wölfl*
Department of Bioanalytics and Molecular Biology
Institute for Pharmacy and Molecular Biology
University of Heidelberg
im Neuenheimer Feld 364, 69120 Heidelberg (Germany)
Tel: (+49) 622-1544-878
E-mail: wolfl@uni-hd.de
Homepage: http://www.uni-heidelberg.de/fakultaeten/biowissenschaften/ipmb/biologie/woelfl/index.html

[b] *V. Pierroz, A. Leonidova, Priv. Doz. Dr. B. Spingler, Prof. Dr. G. Gasser*
Institute of Inorganic Chemistry
University of Zurich, Winterthurerstrasse 190
8057 Zurich (Switzerland)
Tel: (+41) 44-635-46-30
E-mail: gilles.gasser@aci.uzh.ch
Homepage: http://www.gassergroup.com

[c] *V. Pierroz, Priv. Doz. Dr. S. Ferrari*
Institute of Molecular Cancer Research
University of Zurich, Winterthurerstrasse 190
CH-8057 Zurich (Switzerland)

[d] *Dr. A. Pinto, Prof. Dr. N. Metzler-Nolte*
Department of Inorganic Chemistry I-Bioinorganic Chemistry
Faculty of Chemistry and Biochemistry
Ruhr-University Bochum
Universitätsstrasse 150, 44801 Bochum (Germany)
Tel: (+49) 234-322-8152
E-mail: nils.metzler-nolte@rub.de
Homepage: http://www.chemie.rub.de/ac1/

[e] *R. Molteni, Dr. A. Steffen*
Institut für Anorganische Chemie
Julius-Maximilians-Universität Würzburg
Am Hubland, 97074 Würzburg (Germany)
Tel: (+49) 931-318-6180
E-mail: andreas.steffen@uni-wuerzburg.de
Homepage: http://www-anorganik.chemie.uni-wuerzburg.de/forschungsgruppen/dr_a_steffen/

Supporting information for this article is available on the WWW under http://dx.doi.org/10.1002/chem.201304012.

© 2014 Wiley-VCH Verlag GmbH & Co. KGaA, Weinheim

the use of such compounds for medicinal purposes may be rooted in the belief that such compounds are, for example, toxic due to the presence of a metal ion. This conception is erroneous as the toxicity of a metal ion depends on its oxidation state, its coordinated ligands, and obviously on the dose.[1] As proof, it has just to be mentioned that platinum, arsenic, bismuth, gold, antimony, tin, or lutetium complexes are currently in the clinic for the treatment of various medical conditions.[2–6] In addition to all these examples, which are purely coordinative metal complexes—that is, they do not contain any metal–carbon bonds—the antiproliferative, antiparasitic or antibacterial activity of organometallic compounds is currently being intensively investigated by numerous research groups all over the world.[7–15]

In the field of organometallic anticancer drug candidates, ruthenium derivatives have been and are still being intensively investigated.[9,10,13,16–21] Interest in antiproliferative rhenium organometallic complexes, a near neighbor of Ru in the periodic table, is relatively new.[22–37] DNA,[22,23,25–27,31] the side-chains of amino acid residues in peptide and proteins,[22,23] and the active site of enzymes[35] have been proposed as (potential) targets for these Re compounds. It was also demonstrated that rhenium compounds such as $[Re_2(\mu\text{-}OH)_3(CO)_6]^-$, $[Re_2(\mu\text{-}OH)(\mu\text{-}OPh)_2(CO)_6]^-$, $[Re_2(\mu\text{-}OMe)_2(\mu\text{-}dppf)_2(CO)_6]^-$ and $[Re_2(\mu\text{-}OPh)_2(\mu\text{-}dppf)_2(CO)_6]^-$ (dppf = 1,1′-bis(diphenylphosphino)ferrocene) interfere with nucleic acid metabolism at multiple enzyme sites in L1210 lymphoid leukemia cells leading to DNA strand scission.[23,24] Of note, the research groups of Meggers and Gasser have demonstrated that such compounds can be used as photosensitizers for photodynamic therapy purposes.[38,39] Among the different cytotoxic rhenium organometallic complexes studied to date, $Re(CO)_3$ complexes with ligands derived from *N*,*N*′-bis[(quinolin-2-yl)methyl]amine (see L-N_3 in Figure 1 for an

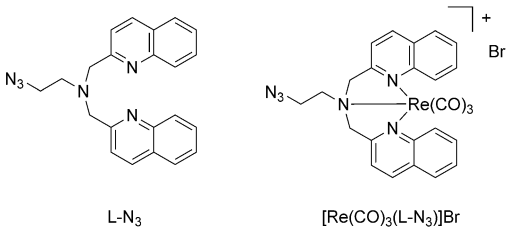

Figure 1. Structures of ligand L-N_3 and of the rhenium tricarbonyl complex of L-N_3 ([$Re(CO)_3$(L-N_3)]Br).

example of such ligands) are of particular interest as they have, in addition to toxicity, luminescent properties enabling cell imaging to be undertaken.[26,27,33] These luminescent properties could potentially help unveil the mode of action of these compounds. Also, the ^{99m}Tc analogues of these $Re(CO)_3$ complexes can usually be easily prepared, as nicely illustrated in the so-called Single Amino Acid Chelate (SAAC) strategy.[40–42] This strategy allows radioimaging to be performed, in addition to fluorescent imaging, and hence to collect important biodistribution data. An example of the synergetic use of related ^{99m}Tc/Re compounds has recently been published by Alberto and co-workers.[35] This team demonstrated that they could synthesize an effective $Re(CO)_3$-containing carbonic anhydrase inhibitor and its ^{99m}Tc analogue.[35] The "cold" Re complex can be used for therapeutic purposes and the "hot" ^{99m}Tc complex for diagnostic purposes, giving an excellent example of theranostic organometallic agents. Such a strategy undoubtedly holds great promise for the future.

Our groups have recently reported the preparation of an azido derivative of this type of ligand (L-N_3, Figure 1) by adapting a synthetic procedure used for a simpler 2,2′-dipicolylamine derivative.[43] Interestingly, the Re tricarbonyl complex of L-N_3, namely [$Re(CO)_3$(L-N_3)]Br (Figure 1), could be used to localize Peptide Nucleic Acid (PNA) oligomers in living cells.[44,45] Inspired by the recent reports by Doyle, Babich, and Zubieta on the cytotoxicity of $Re(CO)_3$ complexes,[26,27,33] we investigated the biological profile of [$Re(CO)_3$(L-N_3)]Br on different cell lines and discovered that [$Re(CO)_3$(L-N_3)]Br was a very cytotoxic compound. Due to this interesting observation, we embarked on a project to obtain more insight into the cytotoxic mode of action of [$Re(CO)_3$(L-N_3)]Br. Since we were also puzzled by the difficulties in imaging bioconjugates of this complex by fluorescence microscopy in living cells,[45] we felt that it was necessary to explore the complexes' photophysical properties in-depth to understand the unusual behavior of [$Re(CO)_3$(L-N_3)]Br, and possibly overcome those obstacles in future studies. Consequently, we now report a detailed study on the photophysical and biological behavior of our rhenium tricarbonyl complex.

Results and Discussion

Synthesis and X-ray crystallography

L-N_3 and [$Re(CO)_3$(L-N_3)]Br were prepared following procedures published by our group.[44] The ligand, L-N_3, could be crystallized by slow evaporation of a hexane solution of L-N_3 at room temperature. L-N_3 crystallizes in the triclinic space group $P\bar{1}$ with one molecule in the asymmetric unit. The X-ray structure of its rhenium tricarbonyl complex has been recently published, now allowing a comparison of both.[44] In the ligand, the two quinoline rings have a dihedral angle of 48.50(4)° relative to each other, compared with 89.7(3)° for the ligand–metal complex (Figure S1a in the Supporting Information). Clearly, this geometrical change is caused by the facial coordination of the ligand to the rhenium. The azide group is nearly linear in the complex (N4–N5 1.220(14), N5–N6 1.110(16), N4-N5-N6 173.1(14) (numbering scheme shown in Figure S1b)), as this is the case for the free ligand (N(26)–N(27) 1.2274(15), N(27)–N(28) 1.1334(16), N(26)-N(27)-N(28) 171.96(14); Figure S1). Further crystallographic details are included in the Supporting Information (Table S1).

Cytotoxic studies

In vitro cytotoxicity assays were performed to obtain an insight into the antitumor activity of [$Re(CO)_3$(L-N_3)]Br; human osteosarcoma (U2OS), human hepatocellular liver (HepG2), and

© 2014 Wiley-VCH Verlag GmbH & Co. KGaA, Weinheim

Table 1. Cytotoxicity expressed as IC_{50} values (μM) with standard deviation. Data were determined as triplicates in three independent experiments.

	U2OS		HepG2		MCF-7	
	CV[a]	Resazurin	CV[a]	Resazurin	CV[a]	Resazurin
2-quinolinecarboxaldehyde	58.5 ± 4.2	44.1 ± 3.4	81.4 ± 1.0	> 100	21.4 ± 0.3	25.6 ± 3.7
L-N_3	> 100	> 100	19.0 ± 2.1	35.3 ± 2.1	9.1 ± 1.4	11.8 ± 0.1
[$ReBr(CO)_5$]	> 100	> 100	> 100	> 100	56.8 ± 0.3	76.9 ± 3.8
[$Re(CO)_3$(L-N_3)]Br	16.4 ± 1.4	16.9 ± 1.5	25.5 ± 0.3	29.8 ± 1.0	6.1 ± 0.1	8.6 ± 0.2
cisplatin	9.0 ± 1.1	8.2 ± 1.5	2.8 ± 0.6	3.9 ± 1.0	1.3 ± 0.1	2.7 ± 0.1

[a] CV = Crystal Violet.

human breast (MCF-7) carcinoma cell lines were used. For comparison purposes, L-N_3, the organometallic rhenium complex [$ReBr(CO)_5$], the known anticancer drug cisplatin, and a quinoline derivative with known antiproliferative properties (2-quinolinecarboxaldehyde)[46] were also screened. Cell viability, which is correlated with the metabolic activity of a cell, was determined by the resazurin assay.[47] Additionally, absolute cell numbers were determined by the Crystal Violet (CV) assay,[48] which can be applied after elution of resazurin. A known number of cells were exposed to increasing concentrations of the different compounds in a 96-well tissue culture plate and incubated for 48 h. IC_{50} values are reported in Table 1. It can be seen that both assays gave similar results although the CV assay generated, in most of the cases, slightly lower IC_{50} values than the resazurin assay.

Generally, with the exception of [$ReBr(CO)_5$], all compounds show antiproliferative activity with IC_{50} values at low or mid-micromolar concentrations for the cell lines investigated in this study. MCF-7 was the most sensitive cell line studied in this work for all compounds. Interestingly, the activity of 2-quinolinecarboxaldehyde and L-N_3 showed a pronounced dependence on the cell line. A similar trend was previously observed in our laboratories with *N*-heterocyclic carbene (NHC) gold compounds.[49] An interesting result of this screening is that the addition of {$Re(CO)_3$} to L-N_3 generates an increase in antitumor activity in U2OS and MCF-7 cells. This observation highlights the synergy needed to engender cell death. A possible explanation for this observation could be an increase in lipophilicity, which allows better uptake of [$Re(CO)_3$(L-N_3)]Br compared with L-N_3. All in all, the interesting cytotoxic profile of [$Re(CO)_3$(L-N_3)]Br incited to us to study its mechanism of action in more detail.

Stability in human plasma

The first study undertaken in our laboratories to unveil the mechanism of action of the rhenium complex was to assess if the observed cytotoxicity was due to [$Re(CO)_3$(L-N_3)]Br itself or due to a decomposition product. For this purpose, we evaluated the stability of the Re complex in human plasma by adapting an experimental procedure recently reported by our group for ferrocenyl derivatives and ruthenium polypyridyl complexes.[50–52] In short, [$Re(CO)_3$(L-N_3)]Br was incubated in human plasma at 37 °C for 0, 24, 48, or 72 h. After extraction, the samples were analyzed by LC-MS. The area of the peak of [$Re(CO)_3$(L-N_3)]Br was compared to the area of the peak corresponding to diazepam, which was used as an internal standard as it is known to not decompose in human plasma. As can be seen in Figure S2 in the Supporting Information, [$Re(CO)_3$(L-N_3)]Br was found to be extremely stable, even after 72 h in human plasma. This finding is a very strong indication that the toxicity observed in cancer cells is due to [$Re(CO)_3$(L-N_3)]Br as a whole.

Photophysical and theoretical studies

To obtain a first insight into the mode of action of the Re organometallic complex, we intended to investigate its cellular localization by fluorescence microscopy, thereby taking advantage of the favorable photophysical properties of the complex.[44] Unfortunately, despite the use of several different experimental conditions, we did not succeed in observing the fluorescence of [$Re(CO)_3$(L-N_3)]Br in living cells. A similar finding had already been observed by our group for a Mn–Re-containing PNA, but was regarded at the time as a singular event.[45] Intrigued by this observation, we decided to investigate more in-depth the photophysical behavior of the complex, experimentally and theoretically, by using DFT and TD-DFT methods.

The absorption, excitation, and emission spectra of [$Re(CO)_3$(L-N_3)]Br were measured in degassed and aerated water and dichloromethane (Figure 2 and Figures S3 and S4 in the Supporting Information). Selected photophysical data are summarized in Table 2. Whereas the previously recorded excitation spectra for the fluorescence (λ_{max} = 430 nm) and phosphorescence (λ_{max} = 560 nm) in ethylene glycol were significantly different from the absorption spectrum, the excitation spectra observed in water or dichloromethane match nicely with the absorption, which shows a maximum at λ_{max}(abs) = 320 nm.[44] It is not clear as yet how ethylene glycol influences the photophysical properties of the rhenium complex, that is, whether the complex undergoes structural changes or partial dissociation of the ligands is enhanced in that solvent.[53] A solvent effect also influences the fluorescence, giving a nicely resolved vibrational pattern in degassed dichloromethane at low concentrations in contrast to the broad emission band in water (see Figures S3 and S4). The excitation of the fluorescence in water shows a maximum at λ = 300 nm, which is slightly shifted to higher energy compared with the excitation maximum of the phosphorescence at λ = 320 nm (Figure S3), indicating that the fluorescence is more efficient when excitation does not occur to S_1, but to a higher-lying Franck–Condon (FC) state (see TD-DFT calculations, vide infra). On the other

© 2014 Wiley-VCH Verlag GmbH & Co. KGaA, Weinheim

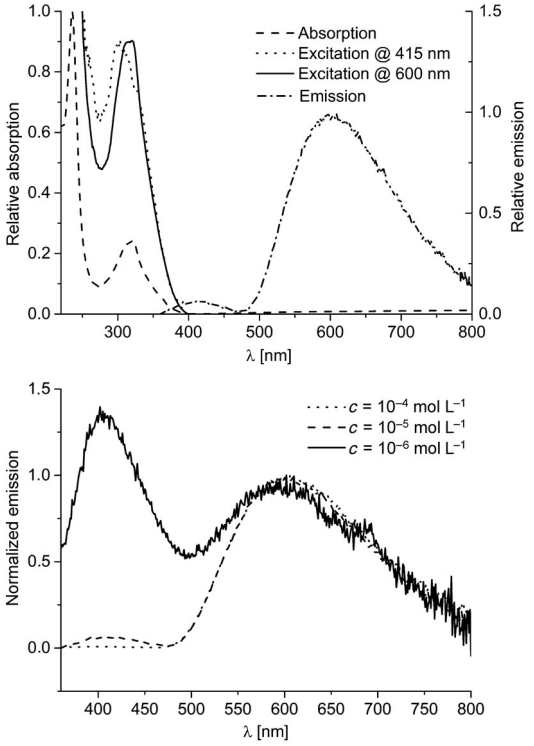

Figure 2. Top: Absorption, emission, and excitation spectra of $[Re(CO)_3(L\text{-}N_3)]Br$ in aerated water. Bottom: Concentration-dependent fluorescence of $[Re(CO)_3(L\text{-}N_3)]Br$ in aerated water.

Table 2. Selected photophysical data for $[Re(CO)_3(L\text{-}N_3)]Br$.

	λ_{abs} [nm]/ ε[L mol^{-1} cm^{-1}]	λ_{em} [nm]	τ [μs]	Φ_p [%]
water (aerated)	232/56900, 320/13500	420, 595	3.54	0.5
water (degassed)[a]			1.25 (6%), 5.22 (94%)	0.8
CH_2Cl_2 (degassed)[b]		405, 575	15.53	2.7

[a] Degassed by bubbling argon through the solution for 20 min. [b] Degassed by freeze-pump-thaw method.

hand, a lower-lying FC singlet state appears to lead most efficiently to the emissive triplet state T_1. However, in dichloromethane this behavior is reversed, that is, the excitation maximum for fluorescence is found at lower energy ($\lambda = 336$ nm) than the excitation maximum for phosphorescence (Figures S3 and S4).

We recognized that the emission band of the fluorescence broadens upon leaving the low concentration solutions over night or after longer exposure to UV light, that is, few hours, and also the excitation spectrum changes. It is possible that additional photophysically active species are formed owing to photodecomposition of the azido group, thereby forming intermediary nitrenes. However, the human plasma experiments tend to indicate that the rhenium complex is stable.

The quantum yields for phosphorescence of $\Phi_p < 0.01$ in degassed and aerated water are very similar and in a typical range for rhenium tricarbonyl bisquinoline complexes (see Table 2).[54,55] The phosphorescence efficiency is greatly enhanced to approximately $\Phi_p = 0.03$ in degassed dichloromethane, indicating a significant solvent effect. However, whereas Φ_p in aerated water remains constant in a concentration range between 10^{-4}–10^{-6} mol L^{-1}, we observed that the fluorescence of $[Re(CO)_3(L\text{-}N_3)]Br$ at $\lambda_{max} = 415$ nm varies, and is fully quenched at high concentrations (Figure 2, right). The fluorescence quenching presumably occurs by resonance energy transfer (RET), owing to the spectral overlap of the emission and the excitation.[56,57] The phosphorescence lifetimes, $\tau_p =$ 5.22–15.53 μs, are similar to those previously reported for related Re diimine and bisquinoline complexes.[54,55] The intrinsic triplet excited state lifetime can be estimated from our lifetime measurements as $\tau_0 = \tau_{obs}/\Phi_p =$ ca. 500 μs, based on the assumptions of photochemical stability and that the observed fluorescence is only residual emission from the S_1 state—a reasonable assumption as intersystem crossing (ISC), $S_1 \rightarrow T_n$, is usually very fast in $[Re(CO)_3L_n]$ complexes and we found high quantum yields for singlet oxygen sensitization of up to $\Phi_D =$ 0.79 for derivatives of $[Re(CO)_3(L\text{-}N_3)]Br$, indicating similar ISC efficiency.[39,58–63] Although the emissive states for fluorescence and phosphorescence have previously been tentatively assigned to be that of intra-ligand (IL) and metal-to-ligand charge transfer (MLCT),[44,55] respectively, we find the intrinsic phosphorescence lifetime relatively long for typical ^{3}MLCT emission, which is usually only a few microseconds for heavy late-transition-metal complexes owing to the strong spin–orbit coupling mediated by the metal atom.[64–67]

For a more detailed description of the photophysical properties of $[Re(CO)_3(L\text{-}N_3)]Br$, we carried out DFT and TD-DFT calculations at the MPW1PW91/LANL2DZ level. All calculations were performed for the gas phase as well as with a conductor polarizable continuum model (CPCM) to describe water as a solvent. The discussion will be focused on the results obtained from the use of the CPCM to ensure a better comparison with the experimental data. The ground-state structure of $[Re(CO)_3(L\text{-}N_3)]Br$ was first optimized, and the structural parameters agree very well with the available data obtained from previous single-crystal X-ray diffraction studies (Table 3).

The molecular orbital diagram in Figure 3 shows the frontier orbital region, and selected orbitals are depicted. The HOMO to HOMO−3 are combinations of the $Re(CO)_3$ fragment, which includes the t_{2g} set of rhenium d orbitals and the π* orbitals of the carbonyl ligands, and the quinoline ligands. The rhenium d orbital participation is most pronounced in the HOMO−3 and HOMO−2, with contributions of approximately 53% (d_{xy}) and 48% (d_{yz}), respectively, whereas the HOMO−1 (21%, d_{xy}) and HOMO (35%, d_{xz}) contain smaller contributions from the metal. The HOMO−5 to HOMO−7 are mainly π-type orbitals located at the quinoline ligands. The LUMO can be found 4.48 eV above the HOMO as an antibonding π* orbital mainly located at the axial quinoline ligand. The same location, although much higher in energy, is true for LUMO+2. In contrast,

© 2014 Wiley-VCH Verlag GmbH & Co. KGaA, Weinheim

Table 3. Selected structural parameters for $[Re(CO)_3(L\text{-}N_3)]Br$ obtained from DFT calculations (MPW1PW91/LANL2DZ).

	CPCM-water		Gas phase		
Structural Parameters	S_0 state	T_1 state	S_0 state	T_1 state	exp.
			bond length [Å]		
Re–N1(amine)	2.244	2.239	2.254	2.247	2.220(8)
Re–N2($quin_{ax}$)	2.228	2.147	2.235	2.130	2.213(8)
Re–N3($quin_{eq}$)	2.230	2.233	2.248	2.238	2.226(8)
Re–C1(*trans* amine)	1.900	1.902	1.903	1.906	1.936(11)
Re–C2(*trans* $quin_{ax}$)	1.902	1.923	1.905	1.933	1.904(10)
Re–C3(*trans* $quin_{eq}$)	1.900	1.907	1.902	1.916	1.940(10)
			bond angle [°]		
C1-Re-C2	87.5	88.3	87.6	88.5	89.9(5)
C1-Re-C3	83.4	84.1	84.0	84.8	86.0(5)
C2-Re-C3	88.3	87.6	88.6	87.7	86.9(4)
N1-Re-N2	73.3	74.2	73.2	74.5	73.2(3)
N1-Re-N3	77.9	77.3	77.3	77.1	78.3(3)
N2-Re-N3	87.3	90.6	89.6	91.8	86.3(3)
N1-Re-C1	171.8	171.2	172.0	171.4	172.0(4)
N2-Re-C2	173.7	174.4	173.3	174.1	171.1(4)
N3-Re-C3	172.4	171.6	171.3	171.1	170.5(4)
			dihedral angle [°]		
$quin_{ax}$-Re-CO(1)	ca. 32	36	31	35	32
$quin_{eq}$-Re-CO(1)	ca. 20	24	20	24	19

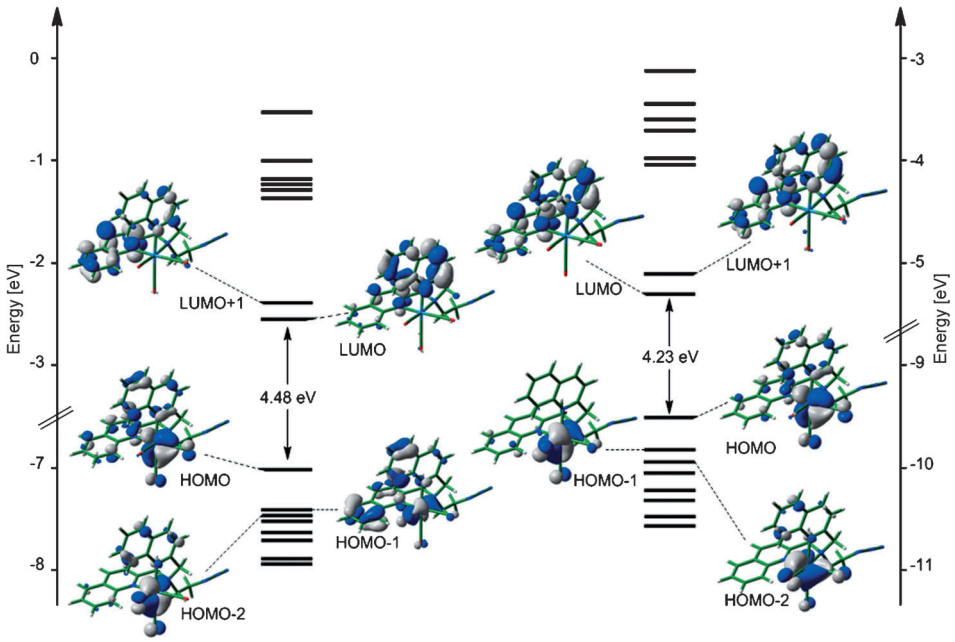

Figure 3. Molecular orbital diagram of the frontier orbital region and Kohn–Sham orbital contour plots (isovalue 0.04) for $[Re(CO)_3(L\text{-}N_3)]Br$, calculated at the MPW1PW91/LANL2DZ level of theory; left: including CPCM-water, right: gas phase.

erate larger MLCT contributions in the excited states (see the Supporting Information). Furthermore, the energy gap between HOMO and HOMO−1/HOMO−2 is smaller. The changes for the virtual orbitals are much less pronounced, leading to a slightly smaller HOMO–LUMO gap of 4.23 eV.

TD-DFT calculations have also been performed from the ground state, S_0, for the first 50 singlet and triplet state excitations (see Table 4 for selected excitations). The major excitations with reasonable oscillator strengths, *f*, that is, $S_1/S_2/S_4 \leftarrow S_0$, lead to ligand-centered (LC) states at 3.66 eV, 3.88 eV, and 4.04 eV, respectively, arising from transitions between HOMO, HOMO−1 and HOMO−2 and the two lowest unoccupied orbitals, LUMO and LUMO+1. Those states contain significant Re(d)-quinoline(π^*) MLCT admixtures, albeit to varying extents (between 34% and 44%). Further into the UV region, the excitations $S_7 \leftarrow S_0$ and $S_8 \leftarrow S_0$, which appear to be (π–π^*) LC/LLCT states, can be found. The calculated UV/Vis absorption spectrum matches nicely with the experimental absorption spectrum, as well as with the experimental excitation spectra of the observed fluorescence (λ_{max} = 420 nm) and of the phosphorescence (λ_{max} = 600 nm) in CH_2Cl_2 or water (Figure 4). The three energetically lowest lying triplet states have been computed at 2.55 eV (FC–T_1), 2.63 eV (FC–T_2), and 3.48 eV (FC–T_3), all of which are primarily of LC/LLCT character, although with some MLCT admixture between 13% and 30%. The higher lying triplet moieties, FC–T_4 to FC–T_7, are mainly ^{3}LC states.

To obtain more insight into the nature of the emitting triplet state and to understand the long lifetimes in combination with low quantum yields, Φ_p, we performed a geometry and energy optimization of the T_1 state by using unrestricted MPW1PW91, with and without a CPCM water model (Table 3). The most pronounced structural change is the shortening of the Re–N($quin_{ax}$) bond by 0.08–0.10 Å and the elongation of the respective *trans* Re–(CO) bond by approximately 0.02 Å. The quinoline ligands are slightly more out-of-plane compared with the ground-state structure. The spin-density distribution in the lowest triplet state, T_1, is depicted in Figure 5, which shows major contributions from the axial quinoline ligand and only minor participation of the Re d_{xz} orbital. Figure 5 also shows the calculated electron density difference between the

LUMO+1 and LUMO+3, also π^*-orbital-type combinations of the aromatic systems, can be found at the equatorial quinoline. It is interesting to see the change in the nature of the molecular orbitals compared to the gas phase calculations, which give the HOMO to HOMO−3 as nearly pure $Re(CO)_3$ fragment orbitals, with Re d_{xz} 44%, Re d_{yz} 59%, Re d_{xy} 55%, and Re d_{xy} 14%, and with hardly any contributions from the quinoline. Consequently, the resulting transitions from these orbitals gen-

© 2014 Wiley-VCH Verlag GmbH & Co. KGaA, Weinheim

Table 4. Selected singlet and triplet excitations from the singlet ground state, S_0, obtained from TD-DFT calculations (MPW1PW91/CPCM-water).

State	Energy [eV]	Energy [nm]	Oscillator strength *f*	Transitions [%][a]	Primary Character
S_1	3.66	339	0.1026	HOMO→LUMO (100)	LC/MLCT(34%)
S_2	3.88	319	0.0989	HOMO→L+1 (100)	LC/MLCT(34%)
S_4	4.04	307	0.0442	H−3→LUMO (33), H−2→LUMO (50), H−1→LUMO (17)	LC/MLCT(44%)
S_7	4.23	293	0.0312	H−2→L+1 (59), H−3→L+1 (18), H−1→L+1 (13)	LC/MLCT(41%)
S_{33}	5.47	227	0.2082	H−2→L+1 (41), H−3→L+1 (27)	LC/MLCT(23%)
S_{34}	5.48	226	0.4737	H−5→L+2 (21), H−1→L+4 (10)	LC/MLCT(14%)
T_1	2.55	486	–	HOMO→LUMO (42), H−1→LUMO (20), H−2–LUMO (10)	LC/MLCT(29%)
T_2	2.63	471	–	HOMO→L+1 (34), H−1→L+1 (24), H−1→LUMO (12)	LC/MLCT(30%)
T_3	3.48	356	–	H−7→LUMO (31), H−7→L+1 (16), H−5→LUMO (22), H-6→LUMO (11)	LC/MLCT(13%)
T_4	3.52	352	–	H−5→L+1 (36), H−7→LUMO (23), H−6→L+1 (17)	LC/MLCT(13%)
T_5	3.67	338	–	HOMO→LUMO (29), H−6→LUMO (25), HOMO→L+4 (10)	LC/MLCT(24%)
T_6	3.71	334	–	H−4→L+5 (58), H−4→L+3 (23), H−4→L+4 (10)	CT(azido)
T_7	3.75	331	–	HOMO→L+1 (43), H−1→LUMO (18)	LC/MLCT(28%)

[a] Major contributions (>10%) only. H=HOMO, L=LUMO.

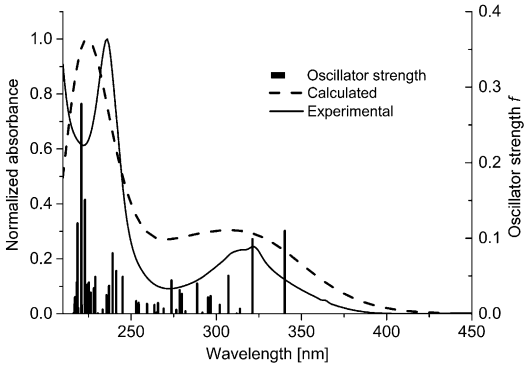

Figure 4. Experimental and calculated (TD-DFT; MPW1PW91/CPCM-water) absorption spectra of $[Re(CO)_3(L\text{-}N_3)]Br$ in water.

lowest triplet state, T_1, and the ground state, S_0, with an energy difference $T_1 \rightarrow S_0$ of approximately 2.10 eV (591 nm), which is in excellent agreement with the experimental value for the phosphorescence (Table 2). Thus, we conclude the emissive T_1 state to be of predominantly ^{3}LC character, an observation that is in contrast to previous assignments of the emitting phosphorescent state as a ^{3}MLCT state.[44,55] Furthermore, the observed fluorescence appears to stem from a ^{1}LC/LLCT state with some MLCT admixture.

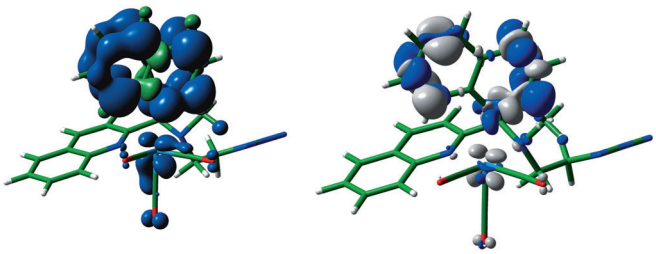

Figure 5. Left: Spin-density distribution in the T_1 state; right: electron-density difference between the lowest triplet state, T_1, and the ground state, S_0. Both structures were obtained from TD-DFT (MPW1PW91/CPCM-water) calculations. Contour plots drawn with an isovalue of 0.002.

Although the emissive lowest energy triplet state contains some MLCT admixture, the coupling with the singlet excited S_n states, allowing phosphorescence to occur through spin–orbit coupling, appears to be weak, as indicated by the very long intrinsic lifetime of the T_1 state (vide supra).[54,64–67] This might be a result of a separation in energy of approximately 0.7 eV between T_1 and S_1 and even higher energy gaps between T_1 and higher lying S_n states, from which the intensity for emission could be borrowed (Table 3). More sophisticated photophysical and theoretical investigations are needed to shed more light on this issue of our specific compounds, but previous reports already indicate that the general photophysical behavior of $Re(CO)_3$-based complexes can be quite complicated.[53,65,68] However, the long intrinsic lifetime of the T_1 state and its dominant ^{3}LC character might be beneficial for further studies on singlet oxygen sensitization, studies that we have carried out on structurally related derivatives of $[Re(CO)_3(L\text{-}N_3)]Br$.[39] In addition, the concentration-dependent fluorescence might be a hint as to why we do not observe emission under certain circumstances in living cells, that is, because of high local concentrations of the rhenium complex (vide infra), although a number of different effects might also be responsible for this phenomenon. For instance, the specific environment of our fluorophore in the cells remains unknown and the experiments with ethylene glycol already indicated that the photophysical properties are highly dependent on the solvent.[44]

Cell death mechanism

To obtain more detailed information on the mechanism of cell death induced by the rhenium complex, we first tested the toxicity and signature markers for apoptotic cell death in the T lymphocyte Jurkat cell line treated with $[Re(CO)_3(L\text{-}N_3)]Br$ (Figure 6). Although Jurkat cells were less sensitive in comparison with U2OS, HepG2, and MCF-7 cells, the sample treated with the highest concentration of $[Re(CO)_3(L\text{-}N_3)]Br$ (40 μM) showed a clear and strong staining with Annexin V after 48 h, indicating induction of apoptosis. Considering the number of

© 2014 Wiley-VCH Verlag GmbH & Co. KGaA, Weinheim

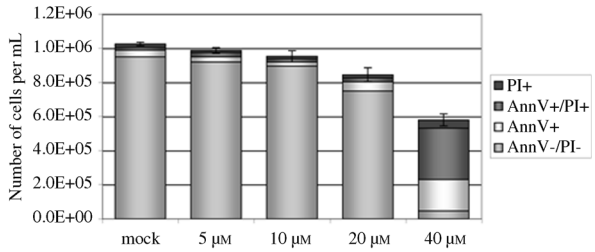

Figure 6. Jurkat cells were treated with the indicated concentrations of $[Re(CO)_3(L\text{-}N_3)]Br$ for 48 h. Cells were counted in a Beckmann Coulter Z2 cell counter and uptake of propidium iodide (PI) and binding of Annexin V was analyzed by flow cytometry (FACS). The results are presented as a relative amount of the total cell number: double negative cells (AnnV−/PI−; viable), Annexin V positive (AnnV+; early apoptotic), Annexin V/PI double positive (AnnV+/PI+; late apoptotic), and PI positive (PI+; dead). Mock is defined as cells treated with solvent only. For presentation results from cell count and relative distribution were combined. Graphs present data from one of three experiments, all showing consistent results.

cells at the beginning of the treatment, an amount that was approximately 30% of the final cell number in the control sample, and the relatively short doubling time of Jurkat cells (25–30 h), the relatively high number of cells counted in the 40 μM sample after 48 h indicates that inhibition of proliferation and apoptosis induction occurred late in treatment.

Induction of the formation of intracellular reactive oxygen species (ROS) is a major hallmark of cell stress and an early indicator of apoptosis in cells.[69] We, therefore, analyzed the level of intracellular ROS in Jurkat cells after 24 and 48 h of treatment by flow cytometry (Figure 7). Our results clearly show a strong and concentration-dependent induction of intracellular ROS. At low concentrations (e.g. 5 and 10 μM of $[Re(CO)_3(L\text{-}N_3)]Br$), only a small and transient enhancement of ROS generation is observed whereas higher concentrations led

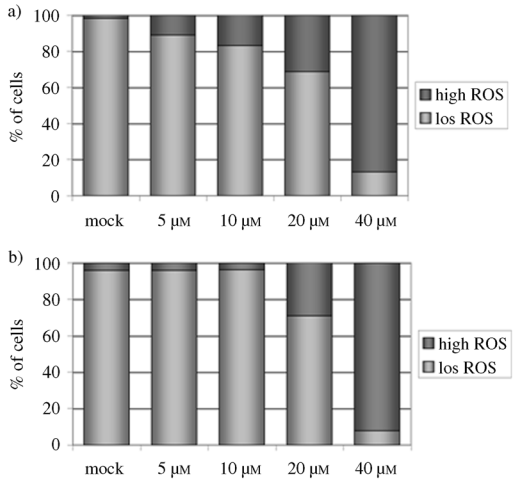

Figure 7. Analysis of intracellular ROS levels in Jurkat cells treated with the indicated concentrations of $[Re(CO)_3(L\text{-}N_3)]Br$ for 24 h (a) and 48 h (b) by FACS. Results are given as percentage of cells with "high" and "low" ROS; "high" and "low" (basal) ROS were defined in corresponding control samples. Graphs present data from one of three experiments, all showing consistent results. Mock is defined as cells treated with solvent only.

to continuously high ROS generation, an observation that is consistent with apoptosis induction.

Another hallmark of apoptosis is the release of cytochrome c from mitochondria.[70] To analyze if mitochondria are a direct target of $[Re(CO)_3(L\text{-}N_3)]Br$ activity, we treated isolated mitochondria from mouse liver cells with $[Re(CO)_3(L\text{-}N_3)]Br$. In this assay (Figure 8), no cytochrome c was released after 1 h of in-

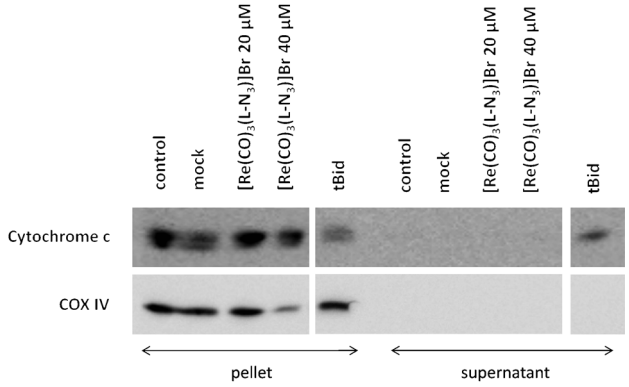

Figure 8. $[Re(CO)_3(L\text{-}N_3)]Br$ does not induce cytochrome c release in isolated mouse-liver mitochondria after 1 h of treatment. COX IV is located in the inner mitochondrial membrane and serves as a marker for mitochondrial localization. tBid, used as a positive control, enhances outer mitochondrial membrane permeability leading to cytochrome c release. Mock is defined as mitochondria treated with solvent only.

cubation with $[Re(CO)_3(L\text{-}N_3)]Br$. Isolated mitochondria were also treated with tBid (truncated Bid) as a positive control. Bid is a pro-apoptotic member of the Bcl-2 family that, upon truncation, translocates to the outer mitochondrial membrane and causes a change in its permeability and the release of cytochrome c.

Influence of $[Re(CO)_3(L\text{-}N_3)]Br$ on cell metabolism

MCF-7 cells were grown on a biosensor chip system in which basic metabolic parameters like glycolysis, respiration, and cell morphology are continuously monitored.[71,72] Treatment of MCF-7 cells with $[Re(CO)_3(L\text{-}N_3)]Br$ immediately reduced cellular respiration by up to 70–75% after 24 h (compared with the respiration rate of untreated cells: 100%) with 10 μM and to 30–40% with 20 μM of $[Re(CO)_3(L\text{-}N_3)]Br$ (Figure 9). Glycolysis was significantly increased, reaching a maximum of a 2-fold increase after 15 h with 20 μM of $[Re(CO)_3(L\text{-}N_3)]Br$. Treatment with 20 μM $[Re(CO)_3(L\text{-}N_3)]Br$ led also to a strong decrease in cell impedance (dark triangles, 20 μM) after about 9 h of treatment, an observation that is typically an indicator of the onset of cell death. A possible explanation for this 9 h induction period before the observed drop in cell impedance could be that the cells have a damage/stress response that triggers a change in cell morphology as well as cell–cell and cell–surface contact. Notably, on the BIONAS biosensor system cells are cultivated at high density, resembling in vivo conditions more closely. Changes in impedance, therefore, occur only at the end-point of cell death. For this reason, concentrations

© 2014 Wiley-VCH Verlag GmbH & Co. KGaA, Weinheim

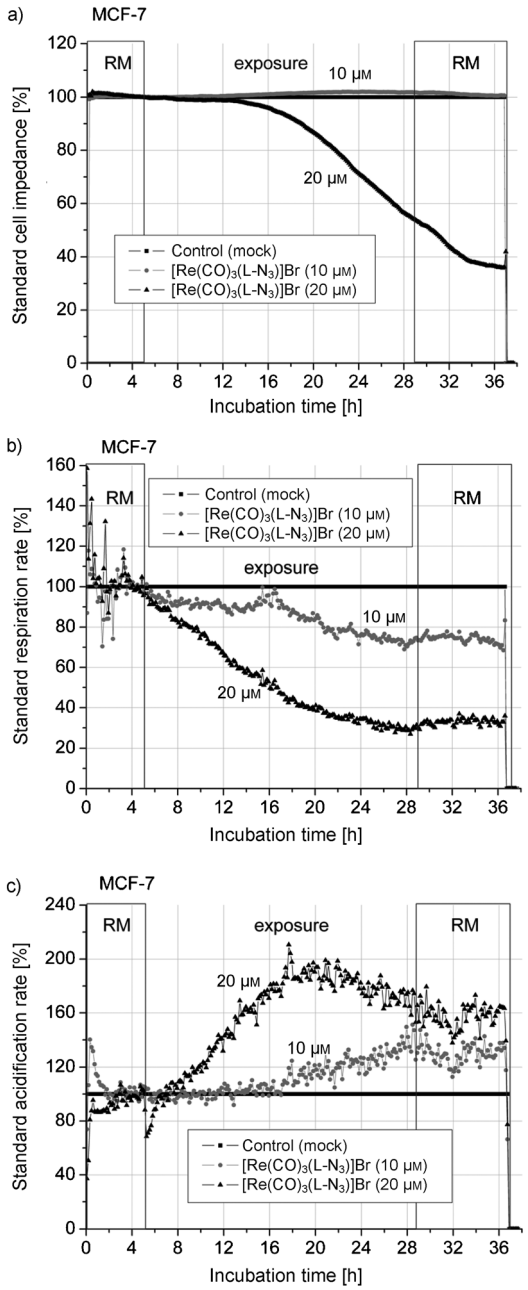

Figure 9. $[Re(CO)_3(L\text{-}N_3)]Br$ immediately inhibits cellular respiration and leads to enhanced glycolysis. MCF-7 cells were treated with 10 and 20 μM $[Re(CO)_3(L\text{-}N_3)]Br$ in the cell biosensor micro-reactor and changes in cell impedance (a), oxygen consumption (respiration; b), and acidification rate (glycolysis; c) are shown relative to untreated control (mock; black line) set to 100%.

higher than the IC_{50} measured in standard cytotoxicity assays are needed. Interestingly, reduced respiratory activity is compensated by increased glycolytic activity. However, later in the treatment, around 15–16 h, exposure to 20 μM of $[Re(CO)_3(L\text{-}N_3)]Br$ reduced the glycolytic activity.[71] These real-time observations clearly indicate the time frame of the induction of cell death in MCF7 cells upon treatment with $[Re(CO)_3(L\text{-}N_3)]Br$. This fits well with the observed late increase in ROS formation and Annexin V staining and suggests that cell death occurs late in the process.

We next asked if this strong effect on cell respiration is a direct effect acting on mitochondria or a secondary effect of the cellular response. We, therefore, investigated the influence of $[Re(CO)_3(L\text{-}N_3)]Br$ on mitochondrial respiration directly by using isolated mitochondria as previously described for other metal complexes.[73–75] For example, Ott et al. recently showed that organometallic gold complexes strongly reduce mitochondrial respiration.[73] Low concentrations of $[Re(CO)_3(L\text{-}N_3)]Br$ (5 and 10 μM) increase oxygen consumption (Figure 10). At 20 μM, a transient increase within the first hour of treatment is observed, followed by an inhibition of respiration after 60 min. Treatment with 40 μM of $[Re(CO)_3(L\text{-}N_3)]Br$ immediately blocks respiration. Of note, Sheldrick and co-workers demonstrated that organorhodium(III) complexes and their organoiridium(III) and trichloridorhodium(III) counterparts have a similar curve of mitochondrial inhibition but not a clear "uncoupling at low concentrations".[75]

Conclusions

There is currently a need for the discovery of novel lead compounds in anticancer research. Owing to their unique physicochemical properties, organometallic complexes offer new opportunities in this field. Metal-specific modes of action have indeed already been unveiled, opening the possibility for overcoming acquired resistance to a previously used drug, as in the case of the antimalarial drug candidate Ferroquine. In this work, we presented an in-depth photophysical and biological study of a Re^{I} organometallic complex, $[Re(CO)_3(L\text{-}N_3)]Br$, which shows cytotoxic activity in the low micromolar range in various cancer cell lines including MCF-7 breast cancer, U2OS osteosarcoma, and HepG2 liver cancer cells. More specifically, we first demonstrated that $[Re(CO)_3(L\text{-}N_3)]Br$ exhibits a concentration-dependent fluorescence, which might be responsible for the observed fluorescence quenching in live cells. In addition, $[Re(CO)_3(L\text{-}N_3)]Br$ shows phosphorescence with quantum yields of up to $\Phi_p = 0.027$ in degassed dichloromethane. Our photophysical and theoretical studies indicate that fluorescence occurs from a ^{1}LC/LLCT state with significant MLCT admixture, whereas the emitting triplet state is predominantly a ^{3}LC state, in contrast to previous assignments. We then discussed in detail the potential cellular targets and the mode of cytotoxic action of $[Re(CO)_3(L\text{-}N_3)]Br$. Towards these aims, we analyzed the immediate effect on cellular metabolism of the Re^{I} compound. Immediately upon addition of $[Re(CO)_3(L\text{-}N_3)]Br$ to MCF-7 breast cancer cells grown on a biosensor-chip microbioreactor, cellular respiration was reduced and glycolysis was increased, indicating a severe shift in cellular metabolism and inhibition of mitochondrial activity. Further analysis of respiration of isolated mitochondria clearly showed that mitochondrial respiratory activity is a direct target of $[Re(CO)_3(L\text{-}N_3)]Br$ and involves two modes of action, namely increased respiration at lower concentrations, potentially through increasing proton transport through the inner mitochondrial membrane, and efficient blocking of respiration at higher concentrations. Interestingly, even low concentrations of the compound are strongly cytotoxic after extended incubation, an observation that could

© 2014 Wiley-VCH Verlag GmbH & Co. KGaA, Weinheim

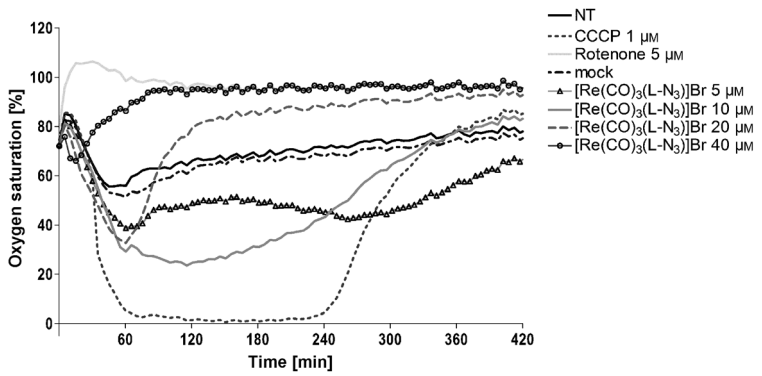

Figure 10. Influence of $[Re(CO)_3(L\text{-}N_3)]Br$ on mitochondrial respiration. Purified mitochondria are maintained in a respiration buffer and oxygen saturation is continuously monitored over time. Rotenone, carbonyl cyanide *m*-chlorophenyl hydrazone (CCCP), and DMSO (mock) are used as controls. Rotenone inhibits complex I of the respiratory chain and completely blocks oxygen consumption. CCCP leads to uncoupling of the oxidative phosphorylation and increases oxygen consumption. $[Re(CO)_3(L\text{-}N_3)]Br$ at low concentrations leads to an initial increase in oxygen consumption, whereas respiration is rapidly blocked at high concentrations.

indicate that proliferation of cells is important for the strong cytotoxic effects observed at low concentrations. All in all, this study sets up the basis for further investigations of $Re(CO)_3$ complexes as novel anticancer drug candidates, especially when taking into account that biodistribution data can be easily achieved by the preparation of the hot ^{99m}Tc analogues of the Re complexes.

Experimental Section

Materials

All reactions were carried out in ordinary glassware and solvents were used without further purification except if indicated. Chemicals were purchased from commercial suppliers and used as received. Solvents were used as received or dried over 4 Å molecular sieves.

Photophysical measurements

UV/Vis absorption spectra and extinction coefficients were obtained on a Hewlett–Packard 8453 diode array spectrophotometer using standard quartz cells with 1 cm path length. Excitation and emission spectra were recorded on an Edinburgh Instrument FLSP920 spectrometer equipped with a 450 W Xenon lamp, double monochromators for the excitation and emission pathways, and a red-sensitive photomultiplier (PMT-R928) as detector. The excitation and emission spectra were fully corrected by using the standard corrections supplied by the manufacturer for the spectral power of the excitation source and the sensitivity of the detector. The quantum yields were measured by use of an integrating sphere with an Edinburgh Instrument FLSP920 spectrometer, following a method described in the literature.[76] The absorbance of the samples was kept below 0.1 to avoid inner filter effects, except for the concentration-dependent measurements, and all measurements were carried out at 293 K. The luminescence lifetimes were measured by using a μF900 pulsed 60W xenon microsecond flashlamp with a repetition rate of 100 Hz and a multichannel scaling module. The emission was collected at right angles to the excitation source with the emission wavelength selected by using a double grated monochromator and detected by a R928-P PMT. The instrument response function (IRF) was measured by using the blank solvent as scattering sample and setting the monochromator at the emission wavelength of the excitation beam. The resulting intensity decay is a convolution of the luminescence decay with the IRF and iterative reconvolution of the IRF with a decay function and non-linear least-squares analysis was used to analyze the convoluted data.

Computational details

DFT calculations were carried out with the Gaussian 09 program.[77] The geometric structures were fully optimized without any symmetry constraint by using the MPW1PW91 functional within the LANL2DZ ECP basis set, augmented by polarization functions for all atoms except hydrogen atoms.[78–81] The unrestricted MPW1PW91 method (UMPW1PW91) was used for the optimization of the lowest energy triplet state. Harmonic vibrational frequency calculations were performed to check that the optimized geometries were energy minima, and the relative energies are zero-point corrected. The solvent was described by the polarizable conductor calculation model (CPCM). TD-DFT calculations were performed at the ground-state geometry for the 50 lowest lying singlet and triplet excited states by using the same functional and basis sets. The isosurface spin-density representations were generated by using the GaussView 5.0 program.[82] Atomic orbital contributions to the molecular orbitals have been determined with the AOMix software package.[83] The determination of percentage of single particle contributions to the vertical excited states was carried out as described in the literature.[84]

X-ray crystallography

Crystallographic data were collected at 183(2) K with $Mo_{K\alpha}$ radiation ($\lambda = 0.7107$ Å) on an Agilent SuperNova, Dual source, with an Atlas detector. A suitable crystal of $L\text{-}N_3$ was covered with the minimal amount of oil (Infineum V8512, formerly known as Paratone N), placed on a nylon loop that was mounted in a CrystalCap Magnetic (Hampton Research), and immediately transferred to the diffractometer. Data were corrected for Lorentz and polarization effects as well as for absorption (numerical). The program suite CrysAlis^{Pro} was used for data collection, multi-scan absorption correction, and data reduction.[85] The structure was solved with direct methods by using SIR97[86] and was refined by full-matrix least-squares methods on F^2 with SHELXL-97.[87] CCDC-960525 ($L\text{-}N_3$) contains the supplementary crystallographic data for this paper. These data can be obtained free of charge from The Cambridge Crystallographic Data Centre via www.ccdc.cam.ac.uk/data_request/cif.

Synthesis and characterization

2-Azido-*N*,*N*-bis[(quinolin-2-yl)methyl]ethanamine ($L\text{-}N_3$): $L\text{-}N_3$ was prepared following the procedure published by our group.[44] The analytical data match with those previously reported.[44] Crystals suitable for X-ray crystallography were obtained by evaporating a solution of $L\text{-}N_3$ in hexane at room temperature.

Rhenium tricarbonyl complex of $L\text{-}N_3$ ($[Re(CO)_3(L\text{-}N_3)]Br$): $[Re(CO)_3(L\text{-}N_3)]Br$ was prepared following the procedure published by our group.[44] The analytical data match with those previously reported.[44]

© 2014 Wiley-VCH Verlag GmbH & Co. KGaA, Weinheim

Cell culture

Human osteosarcoma cells (U2OS) and the human liver hepatocellular carcinoma cell line (HepG2) were cultured in Dulbecco's modified Eagle's medium (DMEM; Gibco) supplemented with 10% fetal calf serum (FCS, Gibco), penicillin (100 U mL^{-1}), streptomycin (100 μg mL^{-1}) at 37 °C and 5% CO_2. The human breast carcinoma MCF-7 cell line was cultured in minimal essential medium (MEM; Gibco) supplemented with 10% FCS (Gibco), L-glutamine (200 mM), penicillin (100 U mL^{-1}), and streptomycin (100 μg mL^{-1}). Jurkat (human acute lymphoblastic leukemia) cells were cultivated and treated in Roswell Park Memorial Institute (RPMI) 1640 medium (PAA laboratories, Austria) supplemented with 10% FCS (PAA) at 37 °C and 5% CO_2.

Cytotoxicity studies

Cytotoxicity studies were performed on three different cell lines, namely U2OS, MCF-7, and HepG2, and cell viability was examined by a fluorometric assay using Resazurin (Promocell GmbH) and cell mass was examined by using the Crystal Violet Assay. In short, one day before treatment the cells were plated in triplicates in 96-well plates at a density of 4×10^3 cells/well in 100 μL of medium. After treatment with the different concentrations of the rhenium complex for 48 h, the medium was removed, and complete medium containing Resazurin (100 μL, 0.2 mg mL^{-1} final concentration) was added. After 4 h of incubation at 37 °C, fluorescence of the highly red fluorescent product Resorufin was quantified at 590 nm (540 nm excitation wavelength) in a SpectraMax M5 microplate Reader. The medium containing Resazurin was then removed and cells were fixed in paraformaldehyde (PFA, 4%) for 15 min at RT for the Crystal Violet Assay. Next, PFA was removed, the cells were washed twice with phosphate buffered saline (PBS), and permeabilized for 5 min at 4 °C with a 0.1% (v/v) Triton X-100 solution in PBS. After permeabilization, cells were incubated with a 0.04% (w/v) aqueous Crystal Violet solution for 1 h with gentle shaking. Excess Crystal Violet was washed twice with double distilled (dd) H_2O. After the plate had been allowed to dry at RT, Crystal Violet was eluted from cells in 96% ethanol overnight at 4 °C. Absorbance was measured at 570 nm in a SpectraMax M5 microplate Reader.

Human plasma stability of ([Re(CO)$_3$(L-N$_3$)]Br)

The human plasma was provided by the Blutspendezentrum, Zurich, Switzerland. [Re(CO)$_3$(L-N$_3$)]Br (1 μL, 20 mM DMSO stock solution) and diazepam (1 μL, 20 mM DMSO stock solution) were added to human plasma (998 μL) and left on a thermoshaker at 37 °C for 0, 24, 48, or 72 h. The compounds were then extracted with CH_2Cl_2/MeOH 10:1 (6 mL) by shaking the samples manually for 15 min and then centrifuging them for 10 min. The organic phase was collected and evaporated under a nitrogen flow. The resulting residue was dissolved in MeOH (200 μL) and analyzed by LC-MS. ESI-MS and LC-MS were recorded by using a Bruker Daltonics HCT 6000 mass spectrometer. LC-MS was performed on an Acquity machine from Waters systems equipped with a photo diode array (PDA) detector, an auto sampler, and a Agilent Zorbax 300SB-C18 analytical column (3.5 μm particle size, 300 Å pore size, 150× 4.6 mm). The LC run (flow rate: 0.5 mL min^{-1}) was done with a linear gradient of A (double distilled water containing 0.1% v/v formic acid) and B (acetonitrile containing 0.1% v/v formic acid); $t=0$ min, 20% B; $t=3$ min, 20% B; $t=17$ min, 100% B; $t=20$ min, 100% B; $t=25$ min, 20% B.

ROS measurements

After treatment with the indicated concentrations of the compound, the cells were collected, washed, and re-suspended (2.5×10^5 cells/0.5 mL) in fluorescence activated cell sorting (FACS) buffer [D-PBS (Gibco) with 1% bovine serum albumin (BSA, PAA laboratories, Austria)]. 1.25 μL of 5 mM dihydroethidium (D1168, Molecular Probes, Invitrogen) solution was added to each sample followed by 15 min incubation at RT in the dark. Signal intensity was analyzed by using a FACS Calibur (Becton Dickinson) and CellQuest Pro (BD) analysis software. Excitation and emission settings were 488 nm and 564–606 nm (FL2 channel), respectively.

Annexin V/PI staining

Jurkat cells were treated with the indicated concentrations of the substance for 48 h, then collected and stained with Annexin V-FITC (Invitrogen) according to the manufacturer's recommendations. In short, approximately 5×10^5 cells were re-suspended in Annexin V staining buffer (50 μL; 10 mM 4-(2-hydroxyethyl)-1-piperazineethanesulfonic acid (HEPES), 140 mM NaCl, and 2.5 mM $CaCl_2$, pH 7.4), Annexin V conjugate (2.5 μL) was added to each probe along with PI solution (1.25 μL, 1 mg mL^{-1}) and the samples were incubated in the dark at room temperature for 15 min. Signal intensity was analyzed by using a FACS Calibur (Becton Dickinson) and CellQuest Pro (BD) analysis software. Excitation and emission settings were 488 nm and 515–545 nm (FL1 channel), respectively, for Annexin V-FITC and 488 nm and 564–606 nm (FL2 channel), respectively, for PI.

Real-time monitoring of cellular metabolism

Continuous monitoring of cell metabolism and morphology was performed by using a Bionas 2500 sensor chip system (Bionas, Rostock, Germany). The sensor chips (SC1000) contain Clark-type electrodes, ion-sensitive field-effect transistors, and two interdigitated electrode structures to measure oxygen consumption, glycolytic rate, and cell–cell and cell–matrix interaction.[88] MCF-7 cells were seeded on the sensor chip and grown in DMEM with penicillin/streptomycin and 10% (v/v) FCS for 24 h in a standard incubator before transfer to the flow-cell unit. After transfer, the medium is continuously exchanged in 8 min cycles (4 min exchange of medium and 4 min without flow), during which the parameters were measured. The running medium (RM) used during analysis was DMEM without carbonate buffer (PAN Cat. Nr. P03-0010) but weakly buffered with HEPES (1 mM) and with reduced FCS (0.1%) and glucose (1 g L^{-1}). Before addition of the compound, the cells on the chip were adjusted to the flow-through conditions with running medium (RM) for 5 h. At the end of each experiment a compound-free step was included with RM, before the cell layer was removed by adding 0.2% Triton X-100 to obtain basic signals without living cells on the sensor surface as a negative control.[71]

Measurement of mitochondrial oxygen consumption

Mitochondria were isolated from mouse liver cells as described earlier.[89] Measurements were performed by using OxoPlate (PreSens, Regensburg, Germany), 96-well plates containing a fluorescence oxygen sensor in each well. Fluorescence is measured in dual mode, with excitation at 540 nm and emissions at 650 nm and at 590 nm for signal and reference. The signal ratio of 650/590 nm corresponds to the oxygen partial pressure. Calibration was performed by using oxygen-free water (1% Na_2SO_3) and air-saturated water. Freshly isolated mitochondria (15–18 μg) were suspended in

© 2014 Wiley-VCH Verlag GmbH & Co. KGaA, Weinheim

Respiration Buffer (100 μL; 25 mM sucrose, 100 mM KCl, 75 mM mannitol, 5 mM $MgCl_2$, 10 mM KH_2PO_4, 0.5 mM EDTA, 10 mM Tris, 0.1% fatty acid-free BSA, pH 7.4) containing pyruvate (10 mM), malate (2 mM), adenosine diphosphate (ADP, 2 mM), and adenosine triphosphate (ATP, 0.5 mM) to activate oxidative phosphorylation. Compounds were added as indicated. Fluorescence was measured continuously over 420 min in 5 min intervals with a Tecan Safire2 plate reader (Tecan, Maennedorf, Switzerland) at 37 °C. Plates were sealed with a breathable membrane (Diversified Biotech, Boston, MA). Controls were performed with rotenone (5 μM, Sigma–Aldrich), an inhibitor of respiratory chain complex I, and carbonyl cyanide 3-chlorophenylhydrazone (CCCP, 1 μM, Sigma–Aldrich) as an uncoupling agent.

Cytochrome c release

Freshly isolated mitochondria (60 μg) from mouse liver cells (20 weeks old, wildtype, C57BL/6) were re-suspended in Respiration Buffer (30 μL, see above) and treated as indicated. Cytochrome c release was analyzed by separating supernatant and mitochondrial pellets by centrifugation for 5 min at 4 °C and 12000 g. Cytochrome c release was analyzed by Western Blot using anti-Cytochrome c antibody and anti-COXIV antibody (both Cell Signaling, Danvers, MA).

Acknowledgements

This work was supported by the Alexander von Humboldt Foundation (fellowship for G.G.), the Swiss National Science Foundation (Professorship No. PP00P2_133568 and Research Grants No. 200021_129910 and No. 200020_146776 for G.G.), the University of Zurich (G.G. and S.F.), the Stiftung für wissenschaftliche Forschung of the University of Zurich (G.G. and S.F.), the Stiftung zur Krebsbekämpfung (S.F.), the Huggenberger-Bischoff Stiftung (S.F.), the University of Zurich Priority Program (S.F.), the Research Department Interfacial Systems Chemistry (fellowship for N.M.-N.), the COST Action CM1105 (G.G. and N.M.-N.), the DFG through the Research Unit "Biological Function of Organometallic Compounds" (FOR 630, http://www.rub.de/for630) (N.M.-N. and S.W.) and the Bavarian State Ministry of Science, Research, and the Arts for the Collaborative Research Network "Solar Technologies go Hybrid" (A.S). A.S. is thankful to Prof. Dr. T. B. Marder for his generous support.

Keywords: anticancer compounds · bioorganometallic chemistry · inorganic chemical biology · luminescence · medicinal organometallic chemistry · rhenium

[1] K. H. Thompson, C. Orvig, *Science* **2003**, *300*, 936 – 939.
[2] J. C. Dabrowiak, *Metals in Medicine*, Wiley, Chichester, **2009**.
[3] J. L. Sessler, S. R. Doctrow, T. J. McMurry, S. J. Lippard, *Medicinal Inorganic Chemistry*, American Chemical Society, Washington, DC, **2005**.
[4] *Bioinorganic Medicinal Chemistry* (Ed.: E. Alessio), Wiley-VCH, Weinheim, **2011**.
[5] *Metallotherapeutic Drugs & Metal-based Diagnostic Agents—The Use of Metals in Medicine* (Eds.: M. Gielen, E. R. T. Tiekink), Wiley, Chichester, **2005**.
[6] N. P. E. Barry, P. J. Sadler, *Chem. Commun.* **2013**, *49*, 5106 – 5131.
[7] G. Jaouen, N. Metzler-Nolte, in *Topics in Organometallic Chemistry, Vol. 32*, Springer, Heidelberg, **2010**.
[8] G. Jaouen, *Bioorganometallics: Biomolecules, Labelling, Medicine*, Wiley-VCH, Weinheim, **2006**.
[9] G. Gasser, I. Ott, N. Metzler-Nolte, *J. Med. Chem.* **2011**, *54*, 3 – 25.
[10] G. Gasser, N. Metzler-Nolte, *Curr. Opin. Chem. Biol.* **2012**, *16*, 84 – 91.
[11] M. Patra, G. Gasser, N. Metzler-Nolte, *Dalton Trans.* **2012**, *41*, 6350 – 6358.
[12] C. G. Hartinger, N. Metzler-Nolte, P. J. Dyson, *Organometallics* **2012**, *31*, 5677 – 5685.
[13] C. G. Hartinger, P. J. Dyson, *Chem. Soc. Rev.* **2009**, *38*, 391 – 401.
[14] P. C. A. Bruijnincx, P. J. Sadler, *Curr. Opin. Chem. Biol.* **2008**, *12*, 197 – 206, and references therein.
[15] C. Biot, D. Dive, in *Medicinal Organometallic Chemistry, Vol. 32* (Eds.: G. Jaouen, N. Metzler-Nolte), Springer, Heidelberg, **2010**, pp. 155 – 193.
[16] G. S. Smith, B. Therrien, *Dalton Trans.* **2011**, *40*, 10793 – 10800.
[17] A. F. A. Peacock, P. J. Sadler, *Chem. Asian J.* **2008**, *3*, 1890 – 1899.
[18] A. M. Pizarro, A. Habtermariam, P. J. Sadler, in *Medicinal Organometallic Chemistry, Vol. 32* (Eds.: G. Jaouen, N. Metzler-Nolte), Springer, Heidelberg, **2010**, pp. 21 – 56, and references therein.
[19] A. Casini, C. G. Hartinger, A. A. Nazarov, P. J. Dyson, in *Medicinal Inorganic Chemistry, Vol. 32* (Eds.: G. Jaouen, N. Metzler-Nolte), Springer, Berlin/Heidelberg, **2010**, pp. 57 – 80.
[20] M. Melchart, P. J. Sadler, in *Bioorganometallics* (Ed.: G. Jaouen), Wiley-VCH, Weinheim, **2006**, pp. 39 – 64.
[21] G. Süss-Fink, *Dalton Trans.* **2010**, *39*, 1673 – 1688, and references therein.
[22] J. Zhang, J. J. Vittal, W. Henderson, J. R. Wheaton, I. H. Hall, T. S. A. Hor, Y.-K. Yan, *J. Organomet. Chem.* **2002**, *650*, 123 – 132.
[23] W. Wang, Y. K. Yan, T. S. A. Hor, J. J. Vittal, J. R. Wheaton, I. H. Hall, *Polyhedron* **2002**, *21*, 1991 – 1999.
[24] Y.-K. Yan, S. E. Cho, K. A. Shaffer, J. E. Rowell, B. J. Barnes, I. H. Hall, *Pharmazie* **2000**, *55*, 307 – 313.
[25] D.-L. Ma, C.-M. Che, F.-M. Siu, M. Yang, K.-Y. Wong, *Inorg. Chem.* **2007**, *46*, 740 – 749.
[26] N. Viola-Villegas, A. E. Rabideau, J. Cesnavicious, J. Zubieta, R. P. Doyle, *ChemMedChem* **2008**, *3*, 1387 – 1394.
[27] N. Viola-Villegas, A. E. Rabideau, M. Bartholom, J. Zubieta, R. P. Doyle, *J. Med. Chem.* **2009**, *52*, 5253 – 5261.
[28] M.-W. Louie, H.-W. Liu, M. H.-C. Lam, T.-C. Lau, K. K.-W. Lo, *Organometallics* **2009**, *28*, 4297 – 4307.
[29] K. K.-W. Lo, M.-W. Louie, K.-S. Sze, J. S.-Y. Lau, *Inorg. Chem.* **2008**, *47*, 602 – 611.
[30] M.-W. Louie, M. H.-O. Lam, K. K.-W. Lo, *Eur. J. Inorg. Chem.* **2009**, *2009*, 4265 – 4273.
[31] J. Ho, W. Y. Lee, K. J. T. Koh, P. P. F. Lee, Y.-K. Yan, *J. Inorg. Biochem.* **2013**, *119*, 10 – 20.
[32] M. D. Bartholomä, A. R. Vortherms, S. Hillier, B. Ploier, J. Joyal, J. Babich, R. P. Doyle, J. Zubieta, *ChemMedChem* **2010**, *5*, 1513 – 1529.
[33] M. D. Bartholomä, A. R. Vortherms, S. Hillier, J. Joyal, J. Babich, R. P. Doyle, J. Zubieta, *Dalton Trans.* **2011**, *40*, 6216 – 6225.
[34] D. K. Orsa, G. K. Haynes, S. K. Pramanik, M. O. Iwunze, G. E. Greco, D. M. Ho, J. A. Krause, D. A. Hill, R. J. Williams, S. K. Mandal, *Inorg. Chem. Commun.* **2008**, *11*, 1054 – 1056.
[35] D. Can, B. Spingler, P. Schmutz, F. Mendes, P. Raposinho, C. Fernandes, F. Carta, A. Innocenti, I. Santos, C. T. Supuran, R. Alberto, *Angew. Chem.* **2012**, *124*, 3410 – 3413; *Angew. Chem. Int. Ed.* **2012**, *51*, 3354 – 3357.
[36] A. Kermagoret, G. Morgant, J. D'Angelo, A. Tomas, P. Roussel, G. Bastian, P. Collery, D. Desmaële, *Polyhedron* **2011**, *30*, 347 – 353.
[37] P. Collery, A. Mohsen, A. Kermagoret, J. D'Angelo, G. Morgant, D. Desmaele, A. Tomas, T. Collery, M. Wei, A. Badawi, *Anticancer Res.* **2012**, *32*, 2769 – 2781.
[38] A. Kastl, S. Dieckmann, K. Wähler, T. Völker, L. Kastl, A. L. Merkel, A. Vultur, B. Shannan, K. Harms, M. Ocker, W. J. Parak, M. Herlyn, E. Meggers, *ChemMedChem* **2013**, *8*, 924 – 927.
[39] A. Leonidova, V. Pierroz, R. Rubbiani, J. Heier, S. Ferrari, G. Gasser, *Dalton Trans.* in press, DOI: 10.1039/C1033DT51817E.
[40] M. Bartholomä, J. Valliant, K. P. Maresca, J. Babich, J. Zubieta, *Chem. Commun.* **2009**, 493 – 512.
[41] K. A. Stephenson, S. R. Banerjee, T. Besanger, O. O. Sogebin, M. K. Levadala, N. McFarlane, J. A. Lemon, D. R. Boreham, K. P. Maresca, J. D. Brennan, J. W. Babich, J. Zubieta, J. F. Valliant, *J. Am. Chem. Soc.* **2004**, *126*, 8598 – 8599.

 © 2014 Wiley-VCH Verlag GmbH & Co. KGaA, Weinheim

[42] K. A. Stephenson, J. Zubieta, S. R. Banerjee, M. K. Levadala, L. Taggart, L. Ryan, N. N. McFarlane, D. R. Boreham, K. P. Maresca, J. W. Babich, J. F. Valliant, *Bioconjugate Chem.* **2004**, *15*, 128 – 136.
[43] G. Gasser, K. Jäger, M. Zenker, R. Bergmann, J. Steinbach, H. Stephan, N. Metzler-Nolte, *J. Inorg. Biochem.* **2010**, *104*, 1133 – 1140.
[44] G. Gasser, A. Pinto, S. Neumann, A. M. Sosniak, M. Seitz, K. Merz, R. Heumann, N. Metzler-Nolte, *Dalton Trans.* **2012**, *41*, 2304 – 2313.
[45] G. Gasser, S. Neumann, I. Ott, M. Seitz, R. Heumann, N. Metzler-Nolte, *Eur. J. Inorg. Chem.* **2011**, 5471 – 5478.
[46] S. Broch, B. Aboab, F. Anizon, P. Moreau, *Eur. J. Med. Chem.* **2010**, *45*, 1657 – 1662, and references therein.
[47] J. O'Brien, I. Wilson, T. Orton, F. Pognan, *Eur. J. Biochem.* **2000**, *267*, 5421 – 5426.
[48] G. Bernhardt, H. Reile, H. Birnbiick, T. Sprufl, H. Schiinenberger, *J. Cancer Res. Clin. Oncol.* **1992**, *118*, 35 – 43.
[49] J. Lemke, A. Pinto, P. Niehoff, V. Vasyleva, N. Metzler-Nolte, *Dalton Trans.* **2009**, 7063 – 7070.
[50] V. Pierroz, T. Joshi, A. Leonidova, C. Mari, J. Schur, I. Ott, L. Spiccia, S. Ferrari, G. Gasser, *J. Am. Chem. Soc.* **2012**, *134*, 20376 – 20387.
[51] M. Patra, K. Ingram, V. Pierroz, S. Ferrari, B. Spingler, J. Keiser, G. Gasser, *J. Med. Chem.* **2012**, *55*, 8790 – 8798.
[52] M. Patra, K. Ingram, V. Pierroz, S. Ferrari, B. Spingler, R. B. Gasser, J. Keiser, G. Gasser, *Chem. Eur. J.* **2013**, *19*, 2232 – 2235.
[53] K. E. Henry, R. G. Balasingham, A. R. Vortherms, J. A. Platts, J. F. Valliant, M. P. Coogan, J. Zubieta, R. P. Doyle, *Chem. Sci.* **2013**, *4*, 2490 – 2495.
[54] R. A. Kirgan, B. P. Sullivan, D. P. Rillema, *Top. Curr. Chem.* **2007**, *281*, 45 – 100.
[55] L. H. Wei, J. W. Babich, W. Ouellette, J. Zubieta, *Inorg. Chem.* **2006**, *45*, 3057 – 3066.
[56] J. R. Lakowicz, *Principles of Fluorescence Spectroscopy*, Kluwer Academic/Plenum, New York, **1999**.
[57] N. J. Turro, V. Ramamurthy, J. C. Scaiano, *Photochem. Photobiol.* **2012**, *88*, 1033 – 1033.
[58] A. M. Blanco-Rodríguez, K. L. Ronayne, S. Zális, J. Sýkora, M. Hof, A. Vlcek, *J. Phys. Chem. A* **2008**, *112*, 3506 – 3514.
[59] A. Cannizzo, A. M. Blanco-Rodriguez, A. El Nahhas, J. Sebera, S. Zális, A. Vlcek, M. Chergui, *J. Am. Chem. Soc.* **2008**, *130*, 8967 – 8974.
[60] A. M. Blanco-Rodríguez, M. Busby, K. Ronayne, M. Towrie, C. Gradinaru, J. Sudhamsu, J. Sýkora, M. Hof, S. Zális, A. J. Di Bilio, B. R. Crane, H. B. Gray, A. Vlcek, Jr., *J. Am. Chem. Soc.* **2009**, *131*, 11788 – 11800.
[61] A. M. Blanco-Rodríguez, M. Towrie, J. P. Collin, S. Zális, A. Vlcek Jr., *Dalton Trans.* **2009**, 3941 – 3949.
[62] R. Czerwieniec, W. J. Finkenzeller, T. Hofbeck, A. Starukhin, A. Wedel, H. Yersin, *Chem. Phys. Lett.* **2009**, *468*, 205 – 210.
[63] A. El Nahhas, C. Consani, A. M. Blanco-Rodriguez, K. M. Lancaster, O. Braem, A. Cannizzo, M. Towrie, I. P. Clark, S. Zális, M. Chergui, A. Vlcek, *Inorg. Chem.* **2011**, *50*, 2932 – 2943.
[64] H. Yersin, *Top. Curr. Chem.* **2004**, *241*, 1 – 26.
[65] R. Baková, M. Chergui, C. Daniel, A. Vlcek, Jr., S. Zális, *Coord. Chem. Rev.* **2011**, *255*, 975 – 989.
[66] H. Yersin, A. F. Rausch, R. Czerwieniec, T. Hofbeck, T. Fischer, *Coord. Chem. Rev.* **2011**, *255*, 2622 – 2652.
[67] P. T. Chou, Y. Chi, M. W. Chung, C. C. Lin, *Coord. Chem. Rev.* **2011**, *255*, 2653 – 2665.
[68] R. Heydová, E. Gindensperger, R. Romano, J. Sýkora, A. Vlcek Jr., S. Zális, C. Daniel, *J. Phys. Chem. A* **2012**, *116*, 11319 – 11329.
[69] N. Zamzami, P. Marchetti, M. Castedo, D. Decaudin, A. Macho, T. Hirsch, S. A. Susin, P. X. Petit, B. Mignotte, G. Kroemer, *J. Exp. Med.* **1995**, *182*, 367 – 377.
[70] X. Liu, C. N. Kim, J. Yang, R. Jemmerson, X. Wang, *Cell* **1996**, *86*, 147 – 157.
[71] H. Alborzinia, S. Can, P. Holenya, C. Scholl, E. Lederer, I. Kitanovic, S. Wölfl, *PLoS One* **2011**, *6*, e19714.
[72] U. Schatzschneider, J. Niesel, I. Ott, R. Gust, H. Alborzinia, S. Wölfl, *ChemMedChem* **2008**, *3*, 1104 – 1109.
[73] R. Rubbiani, S. Can, I. Kitanovic, H. Alborzinia, M. Stefanopoulou, M. Kokoschka, S. Monchgesang, W. S. Sheldrick, S. Wolfl, I. Ott, *J. Med. Chem.* **2011**, *54*, 8646 – 8657.
[74] S. D. Köster, H. Alborzinia, S. Can, I. Kitanovic, S. Wolfl, R. Rubbiani, I. Ott, P. Riesterer, A. Prokop, K. Merz, N. Metzler-Nolte, *Chem. Sci.* **2012**, *3*, 2062 – 2072.
[75] Y. Geldmacher, K. Splith, I. Kitanovic, H. Alborzinia, S. Can, R. Rubbiani, M. A. Nazif, P. Wefelmeier, A. Prokop, I. Ott, S. Wölfl, I. Neundorf, W. S. Sheldrick, *J. Biol. Inorg. Chem.* **2012**, *17*, 631 – 634.
[76] L. Porrès, A. Holland, L. O. Palsson, A. P. Monkman, C. Kemp, A. Beeby, *J. Fluoresc.* **2006**, *16*, 267 – 272.
[77] Gaussian 09 (Revision A.02), M. J. Frisch, G. W. Trucks, H. B. Schlegel, G. E. Scuseria, M. A. Robb, J. R. Cheeseman, G. Scalmani, V. Barone, B. Mennucci, G. A. Petersson, H. Nakatsuji, M. Caricato, X. Li, H. P. Hratchian, A. F. Izmaylov, J. Bloino, G. Zheng, J. L. Sonnenberg, M. Hada, M. Ehara, K. Toyota, R. Fukuda, J. Hasegawa, M. Ishida, T. Nakajima, Y. Honda, O. Kitao, H. Nakai, T. Vreven, J. A. Montgomery, Jr., J. E. Peralta, F. Ogliaro, M. Bearpark, J. J. Heyd, E. Brothers, K. N. Kudin, V. N. Staroverov, R. Kobayashi, J. Normand, K. Raghavachari, A. Rendell, J. C. Burant, S. S. Iyengar, J. Tomasi, M. Cossi, N. Rega, J. M. Millam, M. Klene, J. E. Knox, J. B. Cross, V. Bakken, C. Adamo, J. Jaramillo, R. Gomperts, R. E. Stratmann, O. Yazyev, A. J. Austin, R. Cammi, C. Pomelli, J. W. Ochterski, R. L. Martin, K. Morokuma, V. G. Zakrzewski, G. A. Voth, P. Salvador, J. J. Dannenberg, S. Dapprich, A. D. Daniels, Ö. Farkas, J. B. Foresman, J. V. Ortiz, J. Cioslowski, D. J. Fox, Gaussian, Inc., Wallingford CT, **2009**.
[78] P. J. Hay, W. R. Wadt, *J. Chem. Phys.* **1985**, *82*, 270 – 283.
[79] J. P. Perdew, K. Burke, M. Ernzerhof, *Phys. Rev. Lett.* **1996**, *77*, 3865 – 3868.
[80] J. P. Perdew, K. Burke, Y. Wang, *Phys. Rev. B* **1996**, *54*, 16533 – 16539.
[81] C. Adamo, V. Barone, *J. Chem. Phys.* **1998**, *108*, 664 – 675.
[82] GaussView, Version 5, R. Dennington, T. Keith, J. Millam, Semichem Inc., Shawnee Mission KS, **2009**.
[83] S. I. Gorelsky, AOMix: Program for Molecular Orbital Analysis, http://www.sg-chem.net/, University of Ottawa, **2011**.
[84] R. A. Vogt, T. G. Gray, C. E. Crespo-Hernandez, *J. Am. Chem. Soc.* **2012**, *134*, 14808 – 14817.
[85] Agilent Technologies, CrysAlis^{Pro} Software system, version 1.171.36.24, Oxford, UK, **2012**.
[86] A. Altomare, M. C. Burla, M. Camalli, G. L. Cascarano, C. Giacovazzo, A. Guagliardi, A. G. G. Moliterni, G. Polidori, R. Spagna, *J. Appl. Crystallogr.* **1999**, *32*, 115 – 119.
[87] G. M. Sheldrick, *Acta Crystallogr. Sect. A* **2008**, *64*, 112 – 122.
[88] R. Ehret, W. Baumann, M. Brischwein, M. Lehmann, T. Henning, I. Freund, S. Drechsler, U. Friedrich, M. L. Hubert, E. Motrescu, A. Kob, H. Palzer, H. Grothe, B. Wolf, *Fresenius J. Anal. Chem.* **2001**, *369*, 30 – 35.
[89] R. Rubbiani, I. Kitanovic, H. Alborzinia, S. Can, A. Kitanovic, L. A. Onambele, M. Stefanopoulou, Y. Geldmacher, W. S. Sheldrick, G. Wolber, A. Prokop, S. Woelfl, I. Ott, *J. Med. Chem.* **2010**, *53*, 8608 – 8618.

Received: October 14, 2013
Published online on January 24, 2014

© 2014 Wiley-VCH Verlag GmbH & Co. KGaA, Weinheim